

Micro-scale photon source in a hybrid cQED system

Ming-Bo Chen(陈明博), Bao-Chuan Wang(王保传), Si-Si Gu(顾思思), Ting Lin(林霆), Hai-Ou Li(李海欧), Gang Cao(曹刚)†, and Guo-Ping Guo(郭国平)‡

Citation: Chin. Phys. B, 2021, 30 (**4**): 048507. DOI: 10.1088/1674-1056/abe29b
Journal homepage: http://cpb.iphy.ac.cn; http://iopscience.iop.org/cpb

What follows is a list of articles you may be interested in

A method to extend wavelength into middle-wavelength infrared based on InAsSb/(Al)GaSb interband transition quantum well infrared photodetector

Xuan-Zhang Li(李炫璋), Ling Sun(孙令), Jin-Lei Lu(鲁金蕾), Jie Liu(刘洁), Chen Yue(岳琛), Li-Li Xie(谢莉莉), Wen-Xin Wang(王文新), Hong Chen(陈弘), Hai-Qiang Jia(贾海强), Lu Wang(王禄)

Chin. Phys. B, 2020, 29 (**3**): 038504. DOI: 10.1088/1674-1056/ab6969

Improved carrier injection and confinement in InGaN light-emitting diodes containing GaN/AlGaN/GaN triangular barriers

Li-Wen Cheng(程立文), Jian Ma(马剑), Chang-Rui Cao(曹常锐), Zuo-Zheng Xu(徐作政), Tian Lan(兰天), Jin-Peng Yang(杨金彭), Hai-Tao Chen(陈海涛), Hong-Yan Yu(于洪岩), Shu-Dong Wu(吴曙东), Shun Yao(尧舜), Xiang-Hua Zeng(曾祥华), Zai-Quan Xu(徐仔全)

Chin. Phys. B, 2018, 27 (**8**): 088504. DOI: 10.1088/1674-1056/27/8/088504

Performance enhancement of ZnO nanowires/PbS quantum dot depleted bulk heterojunction solar cells with an ultrathin Al_2O_3 interlayer

Shuaipu Zang(臧帅普), Yinglin Wang(王莹琳), Meiying Li(李美莹), Wei Su(苏蔚), Meiqi An(安美琦), Xintong Zhang(张昕彤), Yichun Liu(刘益春)

Chin. Phys. B, 2018, 27 (**1**): 018503. DOI: 10.1088/1674-1056/27/1/018503

Photoresponse and trap characteristics of transparent AZO-gated AlGaN/GaN HEMT

Chong Wang(王冲), Meng-Di Zhao(赵梦荻), Yun-Long He(何云龙), Xue-Feng Zheng(郑雪峰), Kun Zhang(张坤), Xiao-Xiao Wei(魏晓晓), Wei Mao(毛维), Xiao-Hua Ma(马晓华), Jin-Cheng Zhang(张进成), Yue Hao(郝跃)

Chin. Phys. B, 2016, 25 (**10**): 108504. DOI: 10.1088/1674-1056/25/10/108504

AlGaN/GaN high-electron-mobility transistor with transparent gate by Al-doped ZnO

Wang Chong, He Yun-Long, Zheng Xue-Feng, Ma Xiao-Hua, Zhang Jin-Cheng, Hao Yue

Chin. Phys. B, 2013, 22 (**6**): 068503. DOI: 10.1088/1674-1056/22/6/068503

SPECIAL TOPIC — Quantum computation and quantum simulation

Micro-scale photon source in a hybrid cQED system*

Ming-Bo Chen(陈明博)[1,2], Bao-Chuan Wang(王保传)[1,2], Si-Si Gu(顾思思)[1,2], Ting Lin(林霆)[1,2], Hai-Ou Li(李海欧)[1,2], Gang Cao(曹刚)[1,2,†], and Guo-Ping Guo(郭国平)[1,2,3,‡]

[1] *Key Laboratory of Quantum Information, CAS, University of Science and Technology of China, Hefei* 230026, *China*
[2] *CAS Center for Excellence in Quantum Information and Quantum Physics, University of Science and Technology of China, Hefei* 230026, *China*
[3] *Origin Quantum Computing Company Limited, Hefei* 230026, *China*

(Received 20 November 2020; revised manuscript received 30 December 2020; accepted manuscript online 3 February 2021)

Coherent photon source is an important element that has been widely used in spectroscopy, imaging, detection, and teleportation in quantum optics. However, it is still a challenge to realize micro-scale coherent emitters in semiconductor systems. We report the observation of gain in a cavity-coupled GaAs double quantum dot system with a voltage bias across the device. By characterizing and analyzing the cavity responses to different quantum dot behaviors, we distinguish the microwave photon emission from the signal gain. This study provides a possibility to realize micro-scale amplifiers or coherent microwave photon sources in circuit quantum electrodynamics (cQED) hybrid systems.

Keywords: SQUID array resonator, double quantum dot, electron–photon coupling, photon emission

PACS: 85.35.Be, 42.50.Pq, 42.60.Da **DOI:** 10.1088/1674-1056/abe29b

1. Introduction

As a fundamental physics process in nature, photon–atom interaction is studied in cavity quantum electrodynamics (QED) at the most elementary approach where a single photon interacts with a single atom at single quantum energy level.[1] It has attracted extensive interest in various experimental platforms.[2–5] Coherent photon source is an important application of cavity QED, which is generated from the population inversion of few atoms in a cavity via stimulated emission.[6] Few-emitter lasers have been demonstrated in atomic[7] and solid-state systems.[8–11]

Semiconductor quantum dot (QD) system, with good scalability[12,13] and compatibility with conventional industrial fabrication,[14] is a promising candidate for solid-state quantum information processor. Experiments on photon emission from biased double quantum dots (DQDs) were also performed and measured using microwave resonators.[15,16] More recently, great progress has been achieved in DQD-resonator hybrid circuit QED systems that studies the electron–photon interaction between superconducting resonators and DQD-defined qubits.[17–20] Benefiting from high impedance resonators,[21,22] these circuit QED systems achieve large electron–photon coupling rates and enable high-sensitivity probe of electron dynamics.[23–26]

Here, we report the observation of reflection gain in a hybrid cQED system which results from photon emission by applying a DC voltage bias across the semiconductor double quantum dots.[15] The tunneling between DQD charge states leads to the emission of microwave photons and phonons simultaneously,[27] probed by a high-impedance superconducting resonator. By comparing the reflection spectrum measured in Coulomb blockade with that measured at the hot spot, we distinguish the photon emission from the frequency shift. The study here provides a possibility to realize a coherent photon source in a semiconductor quantum system.[28]

2. Experimental setup

Our device is made up of a 1/4 wavelength superconducting resonator and a gate-defined DQD, as shown in Fig. 1(a). The resonator consists of an array of superconducting quantum interference devices (SQUIDs)[29] with a tunable resonance frequency f_r. Each SQUID contains two Josephson junctions and its inductance is flux-dependent. In this paper, we set the resonator frequency $f_r = 6.758$ GHz with a total decay linewidth, internal loss rate, and external loss rate $(\kappa, \kappa_i, \kappa_e)/2\pi = (58.9, 36.9, 22.0)$ MHz. Due to the high inductance of the SQUID array, the impedance of the resonator $Z_r \approx 1$ kΩ, which is far beyond 50 Ω of the typical coplanar waveguide.

The DQD is defined by top metallic gates labeled by L, P, U, R, and D within a GaAs/AlGaAs heterostructure. Electrons are trapped in the DQD where the electrochemical potentials of the two dots can be modulated by gates L, P, and R. Then

*Project supported by the National Key Research and Development Program of China (Grant No. 2016YFA0301700), the National Natural Science Foundation of China (Grant Nos. 61922074, 11674300, 61674132, 11625419, and 11804327), the Strategic Priority Research Program of the Chinese Academy of Sciences (Grant No. XDB24030601), and the Anhui Initiative in Quantum Information Technologies, China (Grant No. AHY080000).

†Corresponding author. E-mail: gcao@ustc.edu.cn
‡Corresponding author. E-mail: gpguo@ustc.edu.cn

© 2021 Chinese Physical Society and IOP Publishing Ltd

the charge state $|R\rangle$ ($|L\rangle$) can be defined as an excess electron in the right (left) quantum dot. This two-level system can be modeled with the Hamiltonian $H_{\rm DQD} = \varepsilon\tau_z/2 + t_{\rm c}\tau_x$ with energy splitting $\Omega = \sqrt{\varepsilon^2 + 4t_{\rm c}^2}$, where τ_x and τ_z are Pauli matrices, ε is the detuning defined as the energy difference between $|R\rangle$ and $|L\rangle$, and $t_{\rm c}$ is the interdot tunneling rate.

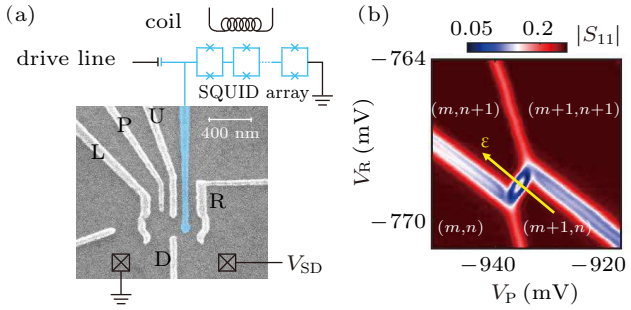


Fig. 1. (a) Scanning electron micrograph of the device. The electrode gates L, P, U, R, and D define the DQD by applying negative bias. A DC voltage $V_{\rm SD}$ can be applied to the source–drain to drive the DQD. The right plunger gate is connected to the SQUID array resonator. The resonator is used to detect the DQD charge state by microwave tone through the drive line. (b) Charge stability diagram of the DQD measured by the SQUID array resonator for $V_{\rm SD} = 0$. The transition between the DQD and source–drain is clearly observed, as well as the interdot transition line with a positive slop.

To couple the DQD to the resonator, the right plunger gate straightforwardly connects to the voltage antinode of the resonator. This hybrid system can be described by the Jaynes–Cummings Hamiltonian[1]

$$H = \Omega\sigma_z/2 + \hbar\omega_{\rm r}a^{\dagger}a + \hbar g_{\rm c}(a^{\dagger}\sigma_- + a\sigma_+), \qquad (1)$$

where σ_z and $\sigma_\pm$ are the Pauli matrices in the DQD eigenstate basis, $\omega_{\rm r} = 2\pi f_{\rm r}$ is the resonator frequency, a and $a^{\dagger}$ are the photon creation and annihilation operators, and $g_{\rm c} = g_0 \cdot 2t_{\rm c}/\Omega$ is the effective coupling strength with the electron–photon coupling rate $g_0/2\pi \approx 57$ MHz which is obtained by fitting the data to the input–output theory.[30,31]

Due to the coupling between the DQD and the resonator, a change of the DQD charge state results in a modification of the susceptibility of the resonator that causes the shift of effective frequency $\Delta f_{\rm r}$. In the dispersive limit, where the energy difference between the resonator and qubit, $\Delta = \Omega - hf_{\rm r}$, is much larger than the coupling rate $g_{\rm c}$, the frequency shift $\Delta f_{\rm r} \propto (g_{\rm c}/\Delta^2)\sigma_z$. Therefore, the DQD charge state can be obtained according to the resonator behavior. In our experiments, we probe the DQD by sending a microwave tone into the SQUID array resonator and measuring the reflected signal. We set the probe frequency $f_{\rm p} = f_{\rm r}$, so the frequency shift leads to an augment in the reflection $|S_{11}|$. Benefiting from the high impedance resonator, the large electron–photon coupling strength enables high-sensitivity probe in our hybrid cQED system.

To perform the experiments, the hybrid device is cooled in a dilution refrigerator with a base temperature of ~ 25 mK. The microwave drive is generated from a vector network analyzer with a power of -30 dBm, passing through an attenuation of ~ 70 dB before reaching the sample. Figure 1(b) shows the stability diagram of the DQD for source–drain bias $V_{\rm SD} = 0$ in the many-electron regime measured in the resonator reflection $|S_{11}|$. The DQD configuration labeled by (m,n) represents m (n) electrons in the left (right) quantum dot.

The stability diagram can be divided into four parts by five tunneling lines. The middle line with a positive slope corresponds to the interdot transition. Along the transition line, the electrochemical potentials of both dots are aligned and the detuning $\varepsilon = 0$. The total electron number in the DQD is unchanged during the tunneling. The other four lines are named charging lines which result from the electron transfer between the two dots and their adjacent reservoir. Two of them have larger linewidth and stronger resonator response that correspond to the electron transfer between the right dot and the reservoir. Because the resonator response to the dot–reservoir tunneling strongly depends on the tunneling rate $\Gamma_{\rm L,R}$, it implies that the coupling of the right dot to the right reservoir $\Gamma_{\rm R}$ is very strong.[32,33]

The probe frequency $f_{\rm p}$ is set on resonance with the resonator, so the measurement of reflected signal $|S_{11}|$ is expected to increase at these tunneling lines. However, except the interdot tunneling, all the charging lines have a smaller reflectance compared to that in Coulomb blockade. This can be explained by the fast decay rate of the charge states induced by the reservoir. The DQD–reservoir electron transfer opens an additional dissipation channel for the hybrid device which deteriorates the resonator quality when the photon interacts with the electron, leading to a larger resonator linewidth and a deeper valley-shaped spectrum at these tunneling lines.

3. Photon emission near hot spot

Generally, a coherent emitter consists of a gain medium, a pumping source, and a resonator. In this cQED hybrid system, the DQD serves as the gain medium. By applying a DC voltage bias across the DQD as a steady pumping source, stimulated photon emission is enabled.

We apply a source–drain bias $V_{\rm SD} = 0.5$ mV to the device, causing sequential electron transfer from the drain to the source. This source–drain bias opens a window for electron tunneling, shown as two finite bias triangles (FBTs) in Fig. 2(a). The two parallel FBTs are encompassed by five tunneling lines. Near the base of each triangle ($\varepsilon \approx 0$), the reflection amplitude is larger than the input, at the position which is called hot spot. To quantify this difference, we define the signal gain as $G = |S_{11}|/|S_{11}^{(\rm c)}|$, where $|S_{11}^{(\rm c)}|$ is the reflection amplitude in deep Coulomb blockade. In deep Coulomb blockade, electron states are far away from the tunneling lines

and deeply trapped in the quantum dot. Therefore, the charge state is barely excited, i.e., $G = 1$.

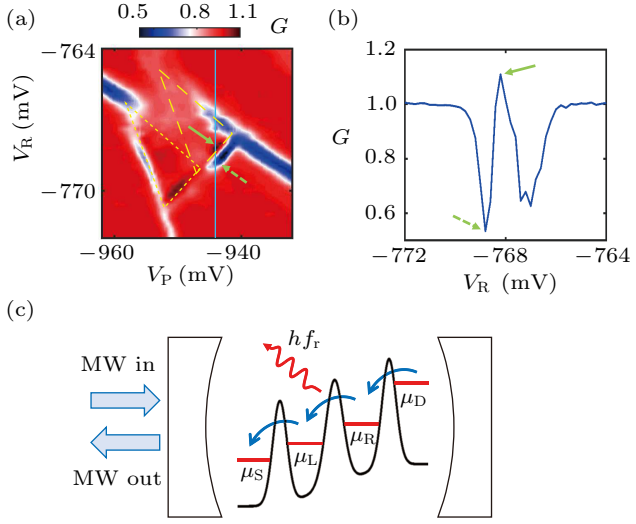


Fig. 2. (a) The gain measured as a function of V_P and V_R with a source–drain bias $V_{SD} = 0.5$ mV. The upper one of the FBTs is outlined with a dashed triangle and the lower one with a dotted triangle. The enhanced reflectance regime with $G > 1$ is indicated by a solid arrow within the FBT while the suppressed reflectance regime with $G < 1$ is indicated by a dashed arrow. (b) A line cut for $V_P = -944$ mV along the vertical line in (a). The peak corresponds to the photon emission while the left valley corresponds to the photon absorption. (c) Schematic diagram of the sequential tunneling dynamics. Electrons jump downhill from the drain to the source and simultaneously emit a microwave photon during interdot tunneing. If the photon frequency matches the resonator frequency, it is caught and stored in the resonator.

In the upper FBT (dashed triangle), the electrochemical potentials of the DQD charge states locate in the bias window and the continuous source–drain pumping enables the sequential tunneling cycle $(m,n) \to (m,n+1) \to (m+1,n) \to (m,n)$. At the hot spot, $\varepsilon > 0$, electrons are loaded into the right dot from the drain, transfer to the left dot, tunnel out of the DQD, finally are repumped by the source–drain bias, following the cycle. Since the potential of the right dot μ_R is higher than that of left μ_L, the energy loss during the interdot transition is converted to a photon and a phonon[27] [Fig. 2(c)]. When the microwave photon matches the resonator frequency, it is stored in the resonator until it decays or is read out from external. On the contrary, if $\varepsilon < 0$, i.e., $\mu_R < \mu_L$, the DQD will absorb a photon and a phonon, tunneling from $|R\rangle$ to $|L\rangle$. As a result, the signal gain $G < 1$ which is indicated by a dashed arrow in Fig. 2(a). Furthermore, the effective DQD–resonator coupling rate in Hamiltonian (1) gives $g_c = g_0 \cdot 2t_c/\Omega$ with $\Omega = \sqrt{\varepsilon^2 + (2t_c)^2}$, which indicates that the electron–photon interaction rate decreases rapidly with increasing $|\varepsilon|$, i.e., the impact of DQD state on the resonator frequency vanishes and G tends to unity for large ε. Therefore, the hot spot only appears near zero detuning in Fig. 2(a).

For a clear comparison between the photon emission and photon absorption, we measure the reflection spectrum $|S_{11}|$ along a vertical line in Fig. 2(a) across the upper FBT, as shown in Fig. 2(b). The spectrum displays two valleys and one peak. The right valley corresponds to the DQD–reservoir tunneling, while the left valley is the result of photon absorption during the interdot transition. The peak reaches maximum of $G = 1.1$ indicated by a solid arrow due to the photon emission from the DQD.

4. Distinguish from frequency shift

In our experiment setup, we take advantage of a 1/4 wavelength SQUID array resonator to couple a semiconductor DQD system and probe the dynamics of the driven DQD. The frequency shift caused by the charge transfer also leads to an increased response of the reflection resonator as explained above, different from the transmission signal of a 1/2 wavelength coplanar waveguide.[15,16] Therefore, we need to distinguish whether the gain observed at the hot spot stems from photon emission or frequency shift.

First, we suppress the photon emission by elevating the interdot potential barrier. The barrier gate voltage V_U is decreased from -900 mV to -1300 mV, so the interdot tunneling rate $2t_c$ is significantly decreased, smaller than the resonator frequency f_r and inhibiting the photon emission. On the other hand, for a smaller $2t_c$, larger energy detuning $\varepsilon = \pm\sqrt{\Omega^2 - (2t_c)^2}$ is required to match the resonance frequency, which weakens the effective coupling strength g_c and suppresses the signal gain of photon emission as well. Figure 3(a) shows the measured reflection $|S_{11}|$ as a function of V_R and V_L for $V_{SD} = 0.5$ mV. The observed gain at the hot spot in Fig. 3(a) results from the frequency shift. To make a better illustration, we compare the frequency spectrum measured at the hot spot (triangle) with that measured in Coulomb blockade (circle) which is served as a baseline. At each spot, the reflection amplitude $|S_{11}|$ is measured as a function of probe frequency f_p, and a small shift is expected as schematically shown in Fig. 3(b). Figure 3(c) shows the measurement result, a zoom-in diagram near the valley of the spectrum. As an evidence of frequency shift caused by the interdot tunneling, the $|S_{11}|$ curve measured at the hot spot is a parallel translation of the baseline. Fitting $|S_{11}|$ to Lorentzian curve, the resonator frequency is shifted by 0.5 MHz. The shift direction depends on the sign of the energy difference $\Delta = \Omega - hf_r$. Since we set the probe frequency on resonance, the small shift leads to an increased response of the resonator. The frequency shift here is so small that the increment $|\Delta S_{11}|/|S_{11}^{(c)}|$ is only about 1.7%.

To obtain the photon emission, we increase V_U back to -900 mV to lift the tunnel barrier. Then the microwave photon emission induced by interdot tunneling is detected by the resonator, and we expect a raise of the spectrum curve compared to the baseline in Coulomb blockade. Similarly, we measure the stability diagram and the spectrum at the hot spot as well as in Coulomb blockade for $V_{SD} = 0.5$ mV, as shown in the lower panel of Fig. 3. In this situation, the observed gain stems from both contributions of frequency shift and photon emission. Despite the obvious upward displacement in Fig. 3(f),

the dashed line (hot spot) also has a small shift compared to the solid line (Coulomb blockade). However, the contribution of frequency shift is very small. After subtracting the contribution of the frequency shift, the increment $|\Delta S_{11}|/|S_{11}^{(c)}| \approx 6.3\%$, quite larger than that caused by the frequency shift (2.9%).

Utilizing the spectra comparison method, we are able to distinguish the photon emission from the enhanced reflected signal at the spot hot. Next, we change the bias window by modulating the source–drain bias from −0.4 mV to 0.4 mV as shown in Fig. 4. The different DC bias voltage directions lead to different shapes of FBTs. The larger voltage, the larger area of bias triangles, and the larger area of hot spot. However, the gain measured for $|V_{SD}| = 0.4$ mV is smaller than that for $|V_{SD}| = 0.2$ mV. This can be explained by the influence of large DQD–reservoir tunneling rate. Because of the larger bias window, electrons with higher energy level and more phonons participate in the cycle $(m,n) \to (m,n+1) \to (m+1,n) \to (m,n)$, which introduce additional decay channel and deteriorate the quantum coherence of the hybrid system. Therefore, fewer photons are conserved when the system reaches balance between the photon emission and photon dissipation.

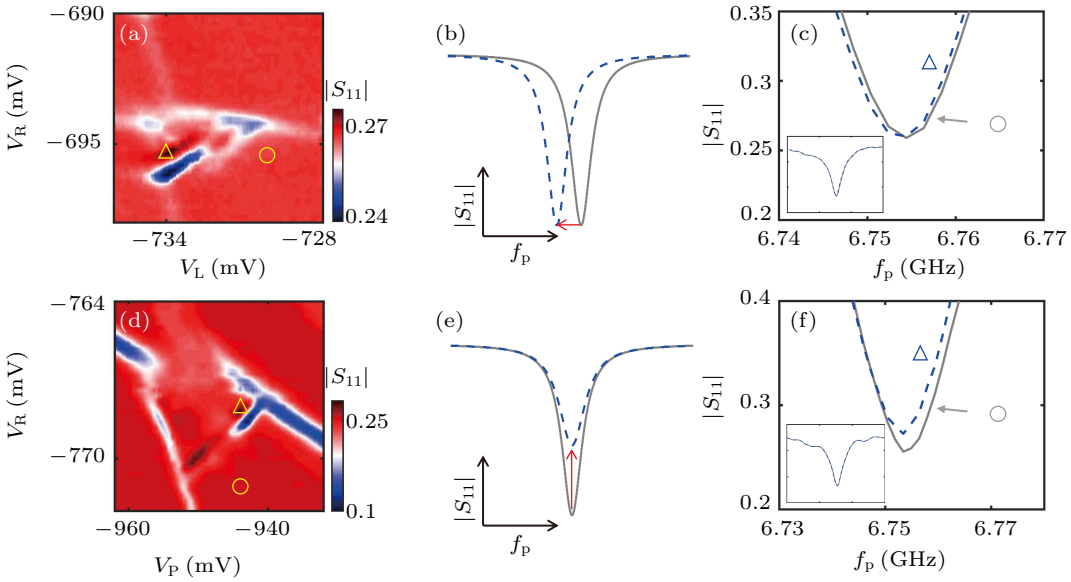


Fig. 3. Distinguish the enhanced reflected signal between photon emission and frequency shift caused by the interdot transition. (a), (d) Stability diagram for $V_{SD} = 0.5$ mV where the hot spot is indicated by a triangle and the Coulomb blockade regime is indicated by a circle. (b), (e) Schematic diagrams illustrate the increased reflections that result from frequency shift and photon emission, respectively. (c), (f) Corresponding zoom-in spectra near the refection valley measured at the hot spot (triangle, dashed line) and Coulomb blockade (circle, solid line). The whole spectrum is shown in the inset.

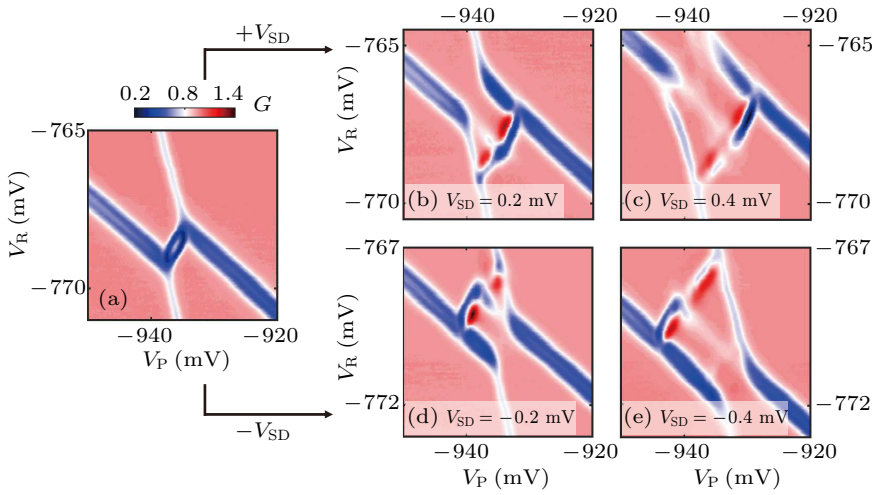


Fig. 4. Photon emission for source–drain bias $V_{SD} = 0$ (a), 0.2 mV (b), 0.4 mV (c), −0.2 mV (d), and −0.4 mV (e).

5. Conclusion

We report the increased cavity response of a SQUID array resonator which results from the photon emission from a semiconductor DQD. Because of the high impedance of the SQUID array resonator, the large coupling strength between the DQD and resonator leads to effective energy transfer between electrons and microwave photons during the interdot tunneling

when a DC voltage bias is consecutively applied across the DQD. By comparing the spectrum measured at the hot spot with the baseline in Coulomb blockade, we distinguish the signal gain caused by photon emission from frequency shift.

In our experiment, the microwave gain of the device is probed in reflection, employing a 1/4 wavelength SQUID array resonator. Compared with a half-wavelength transmission-line resonator, our resonator is designed with smaller footprint, which is advantageous to further on-chip integration with other devices. Furthermore, single-port microwave resonator can suppress the crosstalk between the input and output ports which improves the symmetry of the resonator spectrum.[34,35] Although we have detected the photon emission in the reflection spectrum, the large photon loss rate of the resonator as well as the fast decoherence rate of the DQD deteriorate the measurement. The observed gain at the hot spot is so weak that the photon emission rate is slower than the photon dissipation rate. Therefore, stable stimulated radiation is inaccessible in our voltage-biased DQD system. Provided a resonator and a DQD with better quality and larger coupling strength, we expect the gain will be large enough and coherent photon source will be realized in such hybrid cQED systems.

Acknowledgment

This work was partially carried out at the University of Science and Technology of China Center for Micro- and Nanoscale Research and Fabrication.

References

[1] Walls D F and Milburn G J 2007 *Quantum optics* (Springer Science & Business Media)
[2] Thompson R J, Rempe G and Kimble H J 1992 *Phys. Rev. Lett.* **68** 1132
[3] Brune M, Schmidt-Kaler F, Maali A, Dreyer J, Hagley E, Raimond J M and Haroche S 1996 *Phys. Rev. Lett.* **76** 1800
[4] Kubo Y, Ong F R, Bertet P, Vion D, Jacques V, Zheng D, Dréau A, Roch J F, Auffeves A, Jelezko F, Wrachtrup J, Barthe M F, Bergonzo P and Esteve D 2010 *Phys. Rev. Lett.* **105** 140502
[5] Tabuchi Y, Ishino S, Ishikawa T, Yamazaki R, Usami K and Nakamura Y 2014 *Phys. Rev. Lett.* **113** 083603
[6] Haken H 1983 *Laser Theory* (Springer)
[7] McKeever J, Boca A, Boozer A D, Buck J R and Kimble H J 2003 *Nature* **425** 268
[8] Xie Z G, Götzinger S, Fang W, Cao H and Solomon G S 2007 *Phys. Rev. Lett.* **98** 117401
[9] Nomura M, Kumagai N, Iwamoto S, Ota Y and Arakawa Y 2010 *Nat. Phys.* **6** 279
[10] Astafiev O, Inomata K, Niskanen A, Yamamoto T, Pashkin Y A, Nakamura Y and Tsai J 2007 *Nature* **449** 588
[11] Li Y Y, Liu J Q, Wang T, Liu F Q, Zhai S Q, Zhang J C, Zhou N, Wang L J, Liu S M and Wang Z G 2015 *Chin. Phys. Lett.* **32** 104203
[12] Vandersypen L M K, Bluhm H, Clarke J S, Dzurak A S, Ishihara R, Morello A, Reilly D J, Schreiber L R and Veldhorst M 2017 *npj Quantum Information* **3** 34
[13] Chen Y, Lin F L, Liang X, Jiang N Q 2019 *Chin. Phys. Lett.* **36** 070302
[14] Loss D and DiVincenzo D P 1998 *Phys. Rev. A* **57** 120
[15] Liu Y Y, Petersson K D, Stehlik J, Taylor J M and Petta J R 2014 *Phys. Rev. Lett.* **113** 036801
[16] Stockklauser A, Maisi VF, Basset J, Cujia K, Reichl C, Wegscheider W, Ihn T, Wallraff A and Ensslin K 2015 *Phys. Rev. Lett.* **115** 046802
[17] Samkharadze M, Zheng G, Kalhor N, Brousse D, Sammak A, Mendes U C, Blais A, Scappucci G and Vandersypen L M K 2018 *Science* **359** 1123
[18] Mi X, Benito M, Putz S, Zajac D M, Taylor J M, Burkard G and Petta J R 2018 *Nature* **555** 599
[19] Landig A J, Koski J V, Scarlino P, Mendes U C, Blais A, Reichl C, Wegscheider W, Wallraff A, Ensslin K and Ihn T 2018 *Nature* **560** 179
[20] Cubaynes T, Delbecq M R, Dartiailh M C, Assouly R, Desjardins M M, Contamin L C, Bruhat L E, Leghtas Z, Mallet F, Cottet A and Kontos T 2019 *npj Quantum Information* **5** 47
[21] Samkharadze N, Bruno A, Scarlino P, Zheng G, DiVincenzo D P, DiCarlo L and Vandersypen L M K 2016 *Phys. Rev. Applied* **5** 044004
[22] Wei X Y, Pan J Z, Lu Y P, Jiang L J, Li Z S, Lu S, Tu X C, Zhao Q Y, Jia X Q, Kang L, Chen J, Cao H C, Wang H B, Xu W W, Sun G Z and Wu P H 2020 *Chin. Phys. B* **29** 128401
[23] Zheng G, Samkharadze N,Noordam M L, Kalhor N, Brousse D, Sammak A, Scappucci G and Vandersypen L M K 2019 *Nat. Nanotech.* **14** 742
[24] Hartke T R, Liu Y Y, Gullans M J and Petta J R 2018 *Phys. Rev. Lett.* **120** 097701
[25] Landig A J, Koski J V, Scarlino P, Reichl C, Wegscheider W, Wallraff A, Ensslin K and Ihn T 2019 *Phys. Rev. Lett.* **122** 213601
[26] Chen M B, Wang B C, Kohler S, Kang Y, Lin T, Gu S S, Li H O, Guo G C, Hu X, Jiang H W, Cao G and Guo G P 2020 arXiv:2011.03697 [cond-mat.mes-hall]
[27] Gullans M J, Liu Y Y, Stehlik J, Petta J R and Taylor J M 2015 *Phys. Rev. Lett.* **114** 196802
[28] Liu Y Y, Stehlik J, Eichler C, Gullans M J, Taylor J M and Petta J R 2015 *Science* **347** 285
[29] Stockklauser A, Scarlino P, Koski JV, Gasparinetti S, Andersen CK, Reichl C, Wegscheider W, Ihn T, Ensslin K and Wallraff A 2017 *Phys. Rev. X* **7** 011030
[30] Viennot J J, Dartiailh M C, Cottet A and Kontos T 2015 *Science* **349** 408
[31] Wang B, Lin T, Li H, Gu S, Chen M, Guo G, Jiang H, Hu X, Cao G and Guo G 2021 *Science Bulletin* **66** 332
[32] Frey T, Leek P J, Beck M, Faist J, Wallraff A, Ensslin K, Ihn T and Büttiker M 2012 *Phys. Rev. B* **86** 115303
[33] Li Y, Li S X, Gao F, Li H O, Xu G, Wang K, Liu H, Cao G, Xiao M , Wang T, Zhang J J and Guo G P 2018 *J. Appl. Phys.* **123** 174305
[34] Pompeo N, Torokhtii K, Leccese F, Scorza A, Sciuto S and Silva E 2017 *IEEE International Instrumentation and Measurement Technology Conference*, May 22–25, 2017, Turin, Italy, p. 1
[35] Deng C, Otto M and Lupascu A 2013 *J. Appl. Phys.* **114** 054504